Brightness Asymmetry of Black Hole Images as a Probe of Observer Inclination

Lia Medeiros[1,6] , Chi-Kwan Chan[2,3,4] , Ramesh Narayan[5] , Feryal Özel[2], and Dimitrios Psaltis[2]

[1] School of Natural Sciences, Institute for Advanced Study, 1 Einstein Drive, Princeton, NJ 08540, USA
[2] Steward Observatory and Department of Astronomy, University of Arizona, 933 N. Cherry Avenue, Tucson, AZ 85721, USA
[3] Data Science Institute, University of Arizona, 1230 N. Cherry Avenue, Tucson, AZ 85721, USA
[4] Program in Applied Mathematics, University of Arizona, 617 North Santa Rita, Tucson, AZ 85721, USA
[5] Center for Astrophysics | Harvard & Smithsonian, 60 Garden Street, Cambridge, MA 02138, USA

Abstract

The Event Horizon Telescope recently captured images of the supermassive black hole in the center of the M87 galaxy, which shows a ring-like emission structure with the south side only slightly brighter than the north side. This relatively weak asymmetry in the brightness profile along the ring has been interpreted as a consequence of the low inclination of the observer (around 17° for M87), which suppresses the Doppler beaming and boosting effects that might otherwise be expected due to the nearly relativistic velocities of the orbiting plasma. In this work, we use a large suite of general relativistic magnetohydrodynamic simulations to reassess the validity of this argument. By constructing explicit counterexamples, we show that low inclination is a sufficient but not necessary condition for images to have low brightness asymmetry. Accretion flow models with high accumulated magnetic flux close to the black hole horizon (the so-called magnetically arrested disks) and low black hole spins have angular velocities that are substantially smaller than the orbital velocities of test particles at the same location. As a result, such models can produce images with low brightness asymmetry even when viewed edge on.

Unified Astronomy Thesaurus concepts: Supermassive black holes (1663); Accretion (14); Magnetohydrodynamical simulations (1966)

1. Introduction

The first images of a supermassive black hole at event horizon scale resolution (Event Horizon Telescope Collaboration et al. 2019a, 2019b, 2019c, 2019d, 2019e, 2019f, 2021a, 2021b) have opened a new avenue for studying the characteristics of black holes and their accretion flows. The two main targets of the Event Horizon Telescope (EHT), i.e., the black holes in the center of the M87 galaxy and of our own galaxy (Sagittarius A*, hereafter Sgr A*), are both fed by low-luminosity accretion flows. In this regime, their spectral and imaging properties are best explained in the context of geometrically thick, advection-dominated accretion flows (ADAFs, also called radiatively inefficient accretion flows, RIAFs; see Yuan & Narayan 2014 for a review). As predicted theoretically (Özel et al. 2000) and demonstrated with the EHT images, these flows are optically thin at millimeter wavelengths, and therefore, transparent to synchrotron emission down to the black hole horizon. The millimeter images of these black holes are characterized by a bright ring of emission that surrounds a deep brightness depression: the shadow of the black hole.

The outline of the black hole shadow encodes signatures of the black hole spacetime (see, e.g., Johannsen & Psaltis 2010; Medeiros et al. 2020; Psaltis et al. 2020b). On the other hand, the azimuthal brightness profile of the emission ring carries information primarily about the velocity structure in the accretion flow itself. Relativistic Doppler beaming and boosting causes the re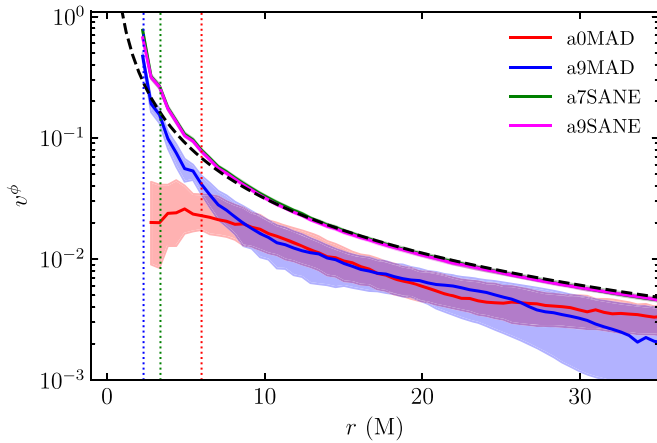gion of the accretion flow with velocities directed toward the observer to appear brighter in the image and the receding side to appear dimmer. As a result, sources that are viewed edge on are expected to have large Doppler asymmetries, and therefore, crescent image shapes; sources that are viewed face on result in a more symmetric ring-link emission structure, as is the case of the M87 image.[7] Such arguments have been used to motivate the use of image brightness asymmetry to measure the inclination of the observer's line of sight with respect to the angular momentum axis of the accretion flow—and also to the spin axis of the black hole, if the latter is assumed to be aligned with the former (Psaltis et al. 2015).

In this paper, we reevaluate the above argument and explore whether it is possible to create an image with low image brightness asymmetry without requiring a low inclination for the observer. Because the asymmetry is caused by relativistic Doppler beaming, a lower angular velocity for the emitting matter could result in significantly lower image brightness asymmetry even at high observer inclinations. Angular velocities that are low compared to the orbital velocities of test particles are frequently seen in the so-called magnetically arrested disks (MADs; see, e.g., Narayan et al. 2012), where magnetic forces close to the black hole alter significantly the angular momentum of the infalling plasma (see also Bronzwaer et al. 2021 for a brief discussion of the lower angular velocities in MAD models). This is contrary to the case of the standard and normal evolution (SANE) models (see, e.g., Igumenshchev et al. 2003) or the semi-analytic models used in Psaltis et al. (2015) (see Figure 1 below and Figure 12 and 20 in Narayan et al. 2012 for a comparison of the angular velocity profiles of MAD and SANE flows). We use the results of detailed

---

[6] NSF Astronomy and Astrophysics Postdoctoral Fellow.

---

[7] Hereafter we will refer to differences in the brightness of the ring as a function of position angle along the ring as image brightness asymmetry to distinguish it from asymmetry in the shape of the ring such as an overall deviation from circularity.

Figure 1. The azimuth- and time-averaged angular velocity (v_ϕ) as a function of radius for the four GRMHD simulations we consider here (the curves for the two SANE simulations are overlapping). The curves show the median while the shaded regions show the 25% and 75% bounds. The black dashed curve corresponds to the Keplerian profile ($v^\phi = r^{-3/2}$). The dotted vertical lines correspond to the location of the innermost stable circular orbit (ISCO) for a black hole with $a_{BH} = 0.0$ (red), $a_{BH} = 0.7$ (green), and $a_{BH} = 0.9$ (blue).

general relativistic magnetohydrodynamic (GRMHD) simulations to show that, indeed, low inclination is not necessary to create images with low image brightness asymmetry. The low plasma velocities near the horizons of low-spin MAD models can create relatively symmetric images even at high observer inclinations. These MAD models are particularly relevant to M87, as they have been shown to be in better agreement with recent EHT polarization results compared to SANE models (Event Horizon Telescope Collaboration et al. 2021a, 2021b). Even though we specifically discuss the implications of our results for the image of the black hole in M87, the image symmetry considerations are more general, and therefore, more broadly applicable.

This paper is organized as follows. In Section 2, we discuss the GRMHD simulation library used in this work. Section 3 discusses how relativistic Doppler effects affect image brightness asymmetry. In Section 4, we introduce a definition for image brightness asymmetry, and in Section 5, we explore how image brightness asymmetry correlates with black hole and accretion flow parameters. We discuss the implications of our work in Section 6 and summarize our findings in Section 7.

2. GRMHD+Radiative Transfer Simulations

We employ a set of GRMHD simulations that were performed using the HARM3D code (Gammie et al. 2003) and that were first discussed in Narayan et al. (2012) and Sądowski et al. (2013). In each simulation, the accretion flow was evolved from a torus located between $r_{in,sim} = 10M$ and $r_{out,sim} = 1000M$ with a peak density around $r_{max} \approx 20M$, and the flow had an adiabatic index of $\gamma = 5/3$. The simulations were run for a long time span, $t = 200{,}000\,GM/c^3$, such that steady state conditions were reached in the inner flows. The set of simulations includes a non-spinning MAD model (hereafter a0MAD), a MAD model with $a_{BH} = 0.9$ (hereafter, a9MAD), a SANE model with $a_{BH} = 0.7$ (hereafter, a7SANE) and a SANE model with $a_{BH} = 0.9$ (hereafter, a9SANE). For more details on the properties of these simulations, see Narayan et al. (2012); and Sądowski et al. (2013).

We perform new radiative transfer and ray-tracing simulations using the fast GPU-based code GRay (Chan et al. 2013).

The code solves the geodesic equations in Boyer–Lindquist coordinates (Psaltis & Johannsen 2012) and integrate the fully covariant radiative transfer equation backward in affine parameter (Younsi et al. 2012). The radiative processes included are thermal synchrotron and bremsstrahlung (Rybicki & Lightman 1986), although synchrotron totally dominates at 1.3 mm. Non-radiative GRMHD simulations are invariant to a rescaling of the number density of the plasma particles but the radiative transfer calculations are not. For this reason, we consider five different values for the number density scale of electrons, for each of these four GRMHD simulations: $n_{e,0} = 10^6\,cm^{-3}$, $5 \times 10^6\,cm^{-3}$, $10^7\,cm^{-3}$, $5 \times 10^7\,cm^{-3}$, and $10^8\,cm^{-3}$, where $n_{e,0}$ corresponds approximately to the number density at horizon scales. We also consider four values for the observer inclination ($i = 0°$, $19°$, $42°$, and $90°$), which are evenly spaced in $\sin i$ given that Doppler effects scale as $v \sin i$.

GRMHD simulations evolve only the internal energy density of the plasma, which allows us to calculate only the temperature of the ions and not of the electrons. We therefore employ a temperature prescription for the electrons that sets the ion-to-electron temperature ratio T_i/T_e based on the local value of the parameter $\beta = P_{gas}/P_{mag}$ (Chan et al. 2015), defined as the ratio of gas pressure to magnetic field pressure, and is given by (Mościbrodzka et al. 2016; Event Horizon Telescope Collaboration et al. 2019d)
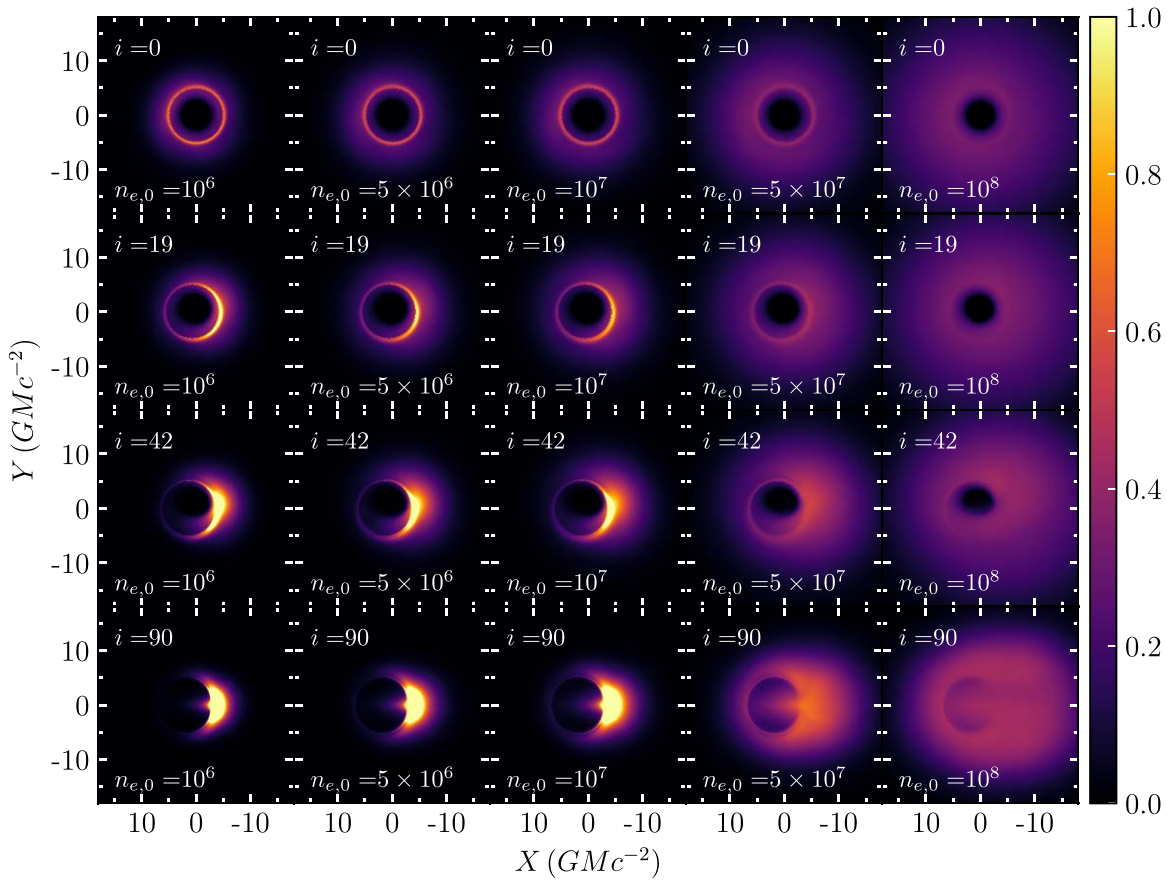
$$\frac{T_i}{T_e} = R_{high}\frac{\beta^2}{1 + \beta^2} + \frac{1}{1 + \beta^2}. \tag{1}$$

We explore three values for the R_{high} parameter ($R_{high} = 1$, 20, and 80)[8] in our suite of simulations.

For the radiative transfer calculations, we further assume a black hole mass of $4.25 \times 10^6 M_\odot$ and a distance of 8.3 kpc. These values were chosen to be consistent with Sgr A* and result in a mass to distance ratio that is comparable to the values measured by the GRAVITY Collaboration and the UCLA Galactic Center Group (see, e.g., Do et al. 2019; Gravity Collaboration et al. 2020, 2021). However, this choice does not limit the generality of our results, because the emissivity of the accretion flow at 1.3 mm approximately depends on the quantity $M_{BH}n_{e,0}^2$, making the black hole mass and the electron number density scale degenerate (see Appendix A of Satapathy et al. 2021; see also Chan et al. 2015). Indeed, when we compare directly our simulations to the M87 results in Section 5, we use a black hole mass of $6.5 \times 10^9 M_\odot$ (Event Horizon Telescope Collaboration et al. 2019a) and shift the range of $n_{e,0}$ values accordingly.

The parameter exploration discussed above resulted in 240 simulations, each with 1024 snapshots with $10GM/c^3$ temporal resolution, a field of view of $64GM/c^2$, and a spatial resolution of $1/8M$ (see Psaltis et al. 2020a for an exploration of optimal pixel resolution). The SANE simulation with spin 0.7 and observer inclination $i = 0°$ was removed from our simulation library due to numerical artifacts caused by the pole of the Boyer–Lindquist coordinate system when viewed at such low inclination. This leaves a total of 225 simulations with 1024 snapshots each for a total of 230,400 image snapshots.

---

[8] Note that a R_{high} value of unity would set the electron temperature equal to the ion temperature, which would result in a model that is unrealistic for the two low-luminosity sources the EHT can resolve. We include these models for consistency with previous work but use $R_{high} = 20$ as our default value.

Figure 2. Effect of changing the electron density scale $n_{e,0}$ (different columns) and the observer inclination i (different rows) on the average image of a SANE simulation with $a_{BH} = 0.9$ spin and $R_{high} = 20$. In all panels the orientation angle of the spin axis on the plane of the sky (ψ) is set to zero so that the black hole spin points upward. Each panel has been normalized such that all panels with the same value of $n_{e,0}$ have the same total flux. The intensity values in the color bar are in arbitrary units. Here and in the following figures, the images were calculated at a wavelength of 1.3 mm and the snapshots were averaged over a time span of $10,240 GMc^{-3}$ with a resolution of $10 GMc^{-3}$.
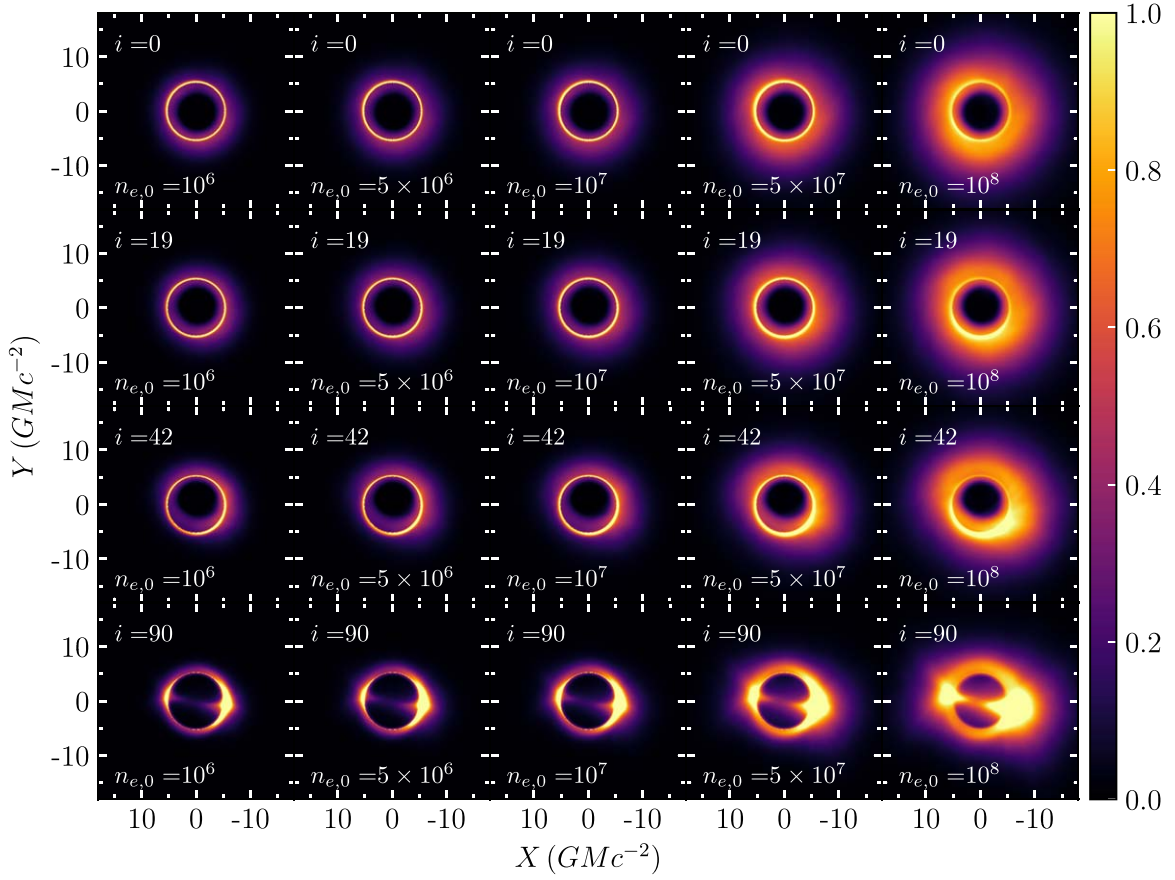
3. Relativistic Doppler Effects in Black Hole Images

In Figure 1 we show the azimuth- and time-averaged angular velocities (v_ϕ) for the four GRMHD simulations we consider. The two SANE simulations follow the Keplerian profile far from the black hole (as expected) and exceed it slightly close to the black hole, as expected. Note that the Keplerian profile shown in the Figure is formally correct only for non-spinning black holes and does not include small spin corrections. Small deviations from the Keplerian profile are expected given the presence of nongravitational forces in the system and even mildly super-Keplerian profiles have been known to appear near transition regions of accretion flows (see, e.g., Abramowicz et al. 1980; Igumenshchev et al. 1998). The non-spinning MAD simulation, however, is significantly below the Keplerian profile and the profile flattens out close to the black hole due to the high magnetic flux. The MAD simulation with spin $a_{BH} = 0.9$ is also significantly below the Keplerian profile far from the black hole but exceeds the Keplerian velocity close to the black hole. The angular velocity for intermediate spin MAD models will fall between these two limits, (see, e.g., Avara et al. 2016, for a MAD model with $a_{BH} = 0.5$ and sub-Keplerian inner disk velocity). Because our simulation library includes a limited sample of spins, we leave a detailed exploration of the dependence of image brightness asymmetry on spin to future work.

Figure 2 shows the effect of changing the electron number density scale and the observer inclination on the average image of the simulations for a representative SANE GRMHD model. Because in this simulation the plasma velocity in the inner accretion flow is comparable to the near-relativistic orbital velocity of test particles, increasing the observer inclination results in a high degree of left-right asymmetry (relative to the angular momentum vector that points upward) due to the Doppler beaming and boosting effects. The plasma on the right side of the shadow moves with very high velocity toward us, causing that side of the image to be substantially brighter than the left, receding side.
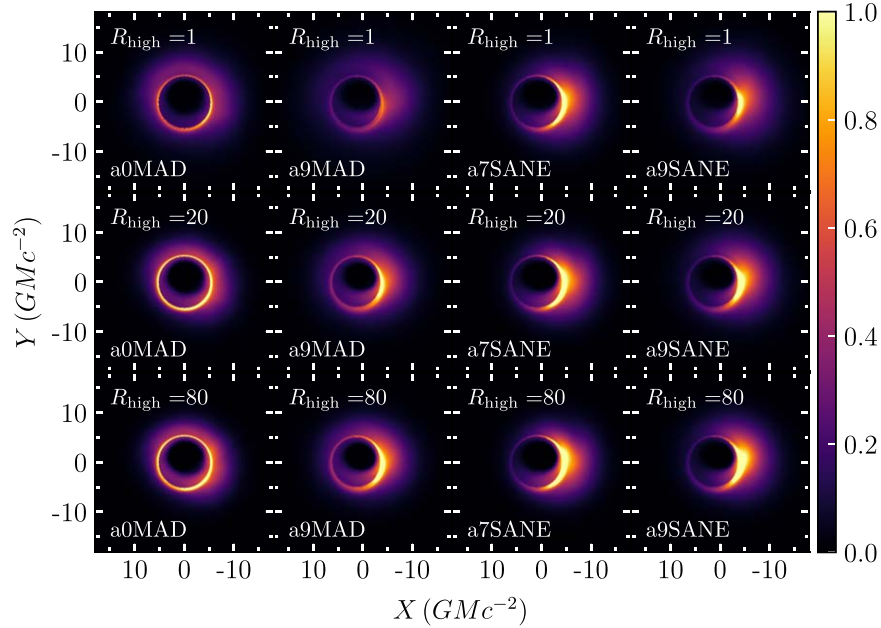
The situation is markedly different in the $a_{BH} = 0$ MAD GRMHD simulation shown in Figure 3, where the left-right brightness asymmetry of the images remains marginal, even at high observer inclinations. This is, of course, a direct consequence of the fact that magnetic stresses at the inner accretion flow substantially reduce the magnitudes of the orbital velocities of the plasmas, and hence, of the Doppler asymmetry of the images.

As expected, increasing the electron number density scale increases the width of the ring in the images (see Satapathy et al. 2021 for a detailed discussion of this effect). As the ring of emission becomes wider, a broader range of annuli in the accretion flow contribute to the image brightness. Originating at larger distances from the horizon, from plasmas with smaller velocities, the photons emerging from such annuli experience a
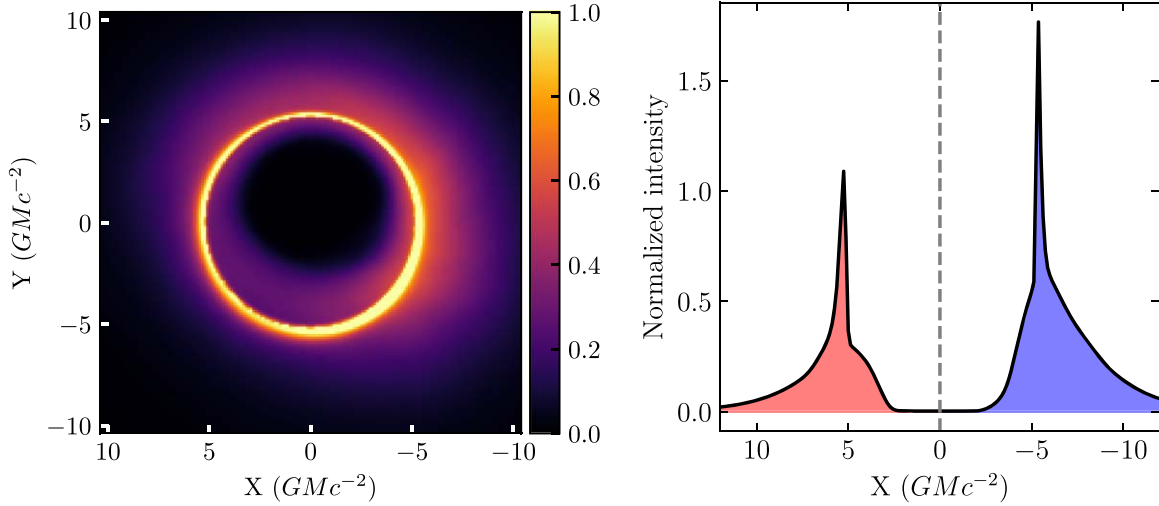
Figure 3. Same as Figure 2 but for a MAD simulation with $a_{\mathrm{BH}} = 0$ spin and $R_{\mathrm{high}} = 20$.

Figure 4. Similar to Figure 3 but showing the effect of changing the ion-to-electron temperature ratio R_{high} (different rows) for four GRMHD simulations. For all models in this figure we have set the electron number density scale to $n_e = 10^7$ cm^{-3}, the inclination to $i = 42°$, and all panels have been normalized such that they have the same total flux.

smaller degree of gravitational lensing and Doppler boosting and the brightness asymmetry of the image is dictated more by the geometric thickness of the flow and projection effects rather than by Doppler effects.

Finally, in Figure 4 we show the effect of changing the ratio of the ion-to-electron temperature R_{high} on the average image of the four simulations for a particular choice of electron number density scale and inclination. Changing R_{high} only has

Figure 5. Left: the average image of a non-spinning MAD simulation with $i = 42°$, $R_{\rm high} = 20$, and $n_{e,0} = 10^7 {\rm cm}^{-3}$. Right: horizontal cross section of the average image shown on the left panel, split into two halves. We define the image brightness asymmetry A as the ratio of the half with the larger integral over X (the shaded blue half in this case) over the half with the smallest integral (the shaded red half in this case). Because of the brightness depression in the center of the image, the exact location of the boundary between the two halves does not significantly affect our asymmetry measure.

a marginal effect on the image brightness asymmetry, as we will quantify in more detail in the next section.
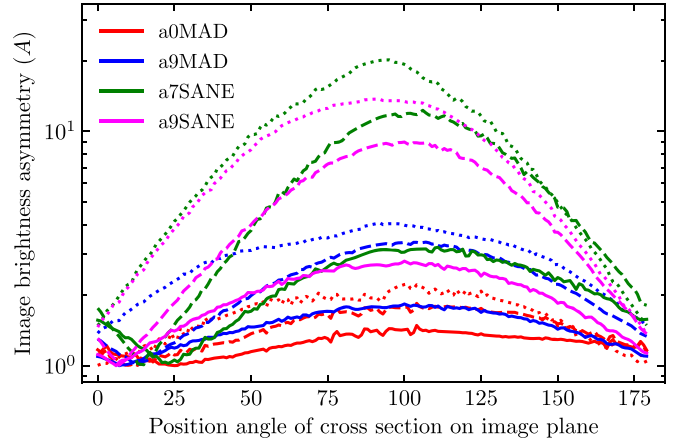
4. Image Brightness Asymmetry

There are numerous approaches one could follow to quantify the brightness asymmetry of a ring-like image, such as decomposing it to polar harmonics or measuring the rms amplitude of its brightness along a circular path. Among the various definitions, we choose here, through trial and error, a particular one that emphasizes the dependence of this asymmetry on the various model parameters.

We start by setting a Cartesian (X,Y) coordinate system on the image plane with the Y-axis parallel to the spin angular momentum of the flow and the black hole, as in Figures 2 and 3. The center of the black hole shadow, and hence, of the image is displaced because of the differential frame dragging effects by $2a_{\rm BH} \sin i$ along the X direction (see, e.g., Bozza et al. 2006; Johannsen & Psaltis 2010). We expect the maximal brightness asymmetry caused by Doppler effects to occur along the $Y = 0$ cross section of the image. For this reason, we consider the brightness of the image along this cross section, which we denote by $I(X, Y = 0)$, and define the brightness asymmetry A as the ratio between the brightness integrated over the two halves of this cross section to the left and to the right of the image center. We further constrain this ratio to be greater than unity by setting the half of the cross section that has the greatest integral as the numerator. This yields

$$ A = \frac{\int_{2a \sin(i)}^{r_{\rm out}} I(X, Y = 0) dX}{\int_{-r_{\rm out}}^{2a \sin(i)} I(X, Y = 0) dX}, \tag{2} $$

if this ratio is larger than unity, or the inverse of it if it is not. In this expression, we have omitted the subscript from $a_{\rm BH}$ for brevity and set $r_{\rm out}$ to the outer radius of the simulated images, which is at $r_{\rm out} = 32 GMc^{-2}$. Equation (2) is defined such that it matches the asymmetry one would measure from a reconstructed black hole image. The definition of A is insensitive to the precise boundary between the two sides of the image, which appears in the limits of the integrals in the numerator and the
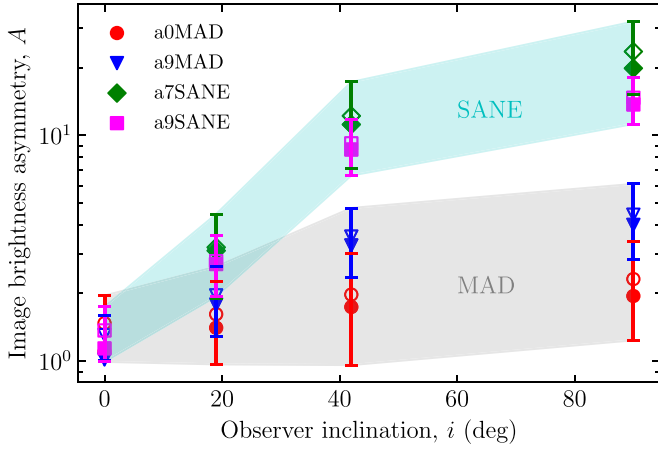

Figure 6. Image brightness asymmetry A calculated along different cross sections on the image plane, at various position angles; a position angle of 90° corresponds to a cross section that is perpendicular to the black hole spin axis. Different colors correspond to the four different GRMHD simulations (with $n_{e,0} = 10^7 {\rm cm}^{-3}$ and $R_{\rm high} = 20$) and different line styles correspond to different observer inclination angles (solid: $i = 19°$; dashed: $i = 42°$; and dotted: $i = 90°$). In all cases we have used the average images of the simulations. The peak image brightness asymmetry occurs for cross sections perpendicular to the black hole spin axis demonstrating that this asymmetry is caused primarily by relativistic Doppler effects.

denominator because of the extended brightness depression at the center of the image.

Figure 5 shows, as an illustrative case, the average image of a non-spinning MAD model and the cross section of the image that is perpendicular to the spin axis of the black hole. In this example, applying our definition of the image brightness asymmetry yields the ratio of the integral of the blue shaded region to the integral of the red shaded region. Because this particular model is for a non-spinning black hole, the center of the image is at $X = 0$.

As a demonstration that the brightness asymmetry is caused by Doppler effects, and therefore, is maximized along the $Y = 0$ cross section, Figure 6 shows the magnitude of asymmetry A but calculated along different cross sections at various position angles with respect to the X-axis. In other words, a position

Figure 7. Image brightness asymmetry as a function of observer inclination angle for all simulations in our set with $n_{e,0} = 10^7$ cm^{-3} and $R_{high} = 20$. Here and in the following figures, filled markers correspond to the image brightness asymmetry of the mean image of that simulation and empty markers and error bars correspond to the mean and standard deviation of the distribution of image brightness asymmetry calculated for each snapshot in the simulations. All models show increased brightness asymmetry with inclination, as expected for Doppler effects. The degree of asymmetry at high inclinations, however, is markedly different between the SANE (cyan shaded region) and the MAD (gray shaded region) models.
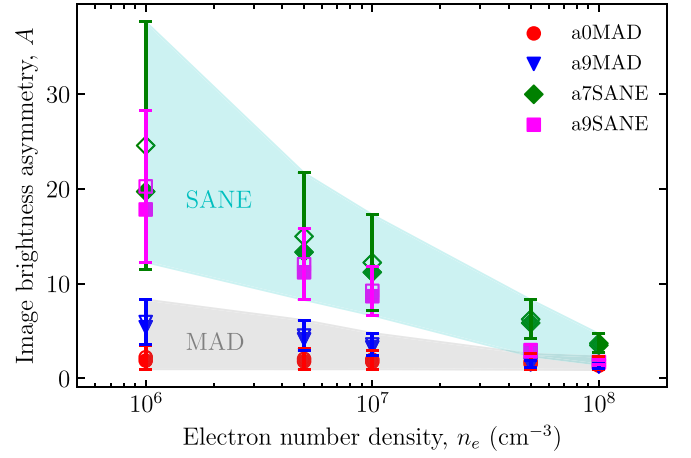

Figure 8. Image brightness asymmetry as a function of the electron number density scale $n_{e,0}$ for all simulations in our set with $i = 42°$ and $R_{high} = 20$.

Figure 9. Image brightness asymmetry as a function of R_{high} for all simulations in our set with $n_e = 10^7$ and $i = 42°$.

angle of 90° corresponds to a cross section that is perpendicular to the black hole spin axis. The various curves correspond to the mean image of all four GRMHD models at different inclination angles. For all simulations that have an inclination $\geqslant 0°$, the maximum brightness asymmetry indeed occurs for position angles $\simeq 90°$.

The non-spinning MAD model is an exception to the above argument, as the mean images in this simulation have a peak asymmetry that is slightly offset from 90° (see, e.g., Figure 3). Coherent asymmetries in the flow can arise from the buoyancy of the magnetic fields in the disk and can remain stable over several dynamical timescales at the large radii that feed the inner accretion flow. Even though this simulation was run for a long time span, there is some persistent asymmetry in the flow parameters (e.g., n_e, B, and β) above and below the $\theta = \pi/2$ plane, which results in the slight offset seen in Figure 3.
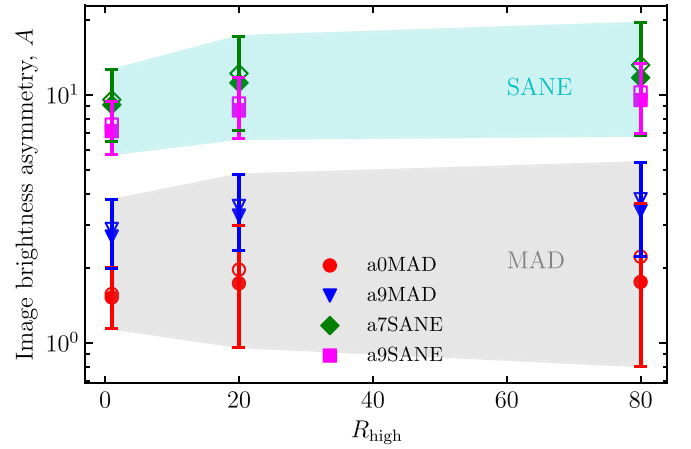
5. Correlations Between Image Brightness Asymmetry and Model Parameters

In order to explore the dependence of image brightness asymmetry on the various parameters of the models and of the black hole, we have calculated it for all of the individual 1024 snapshots of each simulation as well as for all mean images of each simulation. Figure 7 shows the image brightness asymmetry as a function of the inclination angle of the observer, both for the mean images and for the individual snapshots. Even though there is some appreciable variance in the asymmetry between snapshots of the same simulation caused by the turbulent nature of the flow, the difference between MAD and SANE models as well as the dependence of the brightness asymmetry on the observer inclination introduce substantially larger variations. Indeed, the asymmetry in the mean images of each simulation provides an accurate measure of the typical asymmetry found in the individual snapshots.

At each inclination, SANE models have consistently higher asymmetry than the two MAD models, as expected by the fact that the plasma velocities in the former are significantly larger

than in the latter (see also Figures 8 and 9). For the same reason, the brightness asymmetry of the SANE models increases significantly with observer inclination, whereas the MAD models maintain relatively low asymmetry even at high inclinations. In fact, the non-spinning MAD model viewed edge on has an asymmetry that is ~10 times lower than the SANE models viewed at the same inclination. This figure serves as a demonstration of the fact that an image with low brightness asymmetry does not require low observer inclination. On the other hand, if high asymmetry is observed over several epochs, it will be indicative of not only a high inclination but also of the presence of large azimuthal plasma velocities.

Figure 8 shows the dependence of image brightness asymmetry on the electron number density scale $n_{e,0}$. As discussed earlier, when the electron number density increases in the flow, so does the width of the ring in the image. Thicker rings result in more symmetric images since the Doppler effects and lensing effects are less dominant in determining the image structure. It is interesting that the variance in the brightness asymmetry between the snapshots of the various simulations increases with decreasing value of the electron number density scale, especially for the SANE models. This is expected because, when the ring width in the image is small, localized turbulent perturbations in the plasma emission from regions

with high velocities cause substantial brightness changes in the image. On the other hand. when the ring width in the image is large and the emission is coming also from regions of smaller plasma velocities, the effect of several localized perturbations is averaged out and the brightness asymmetry becomes less variable.
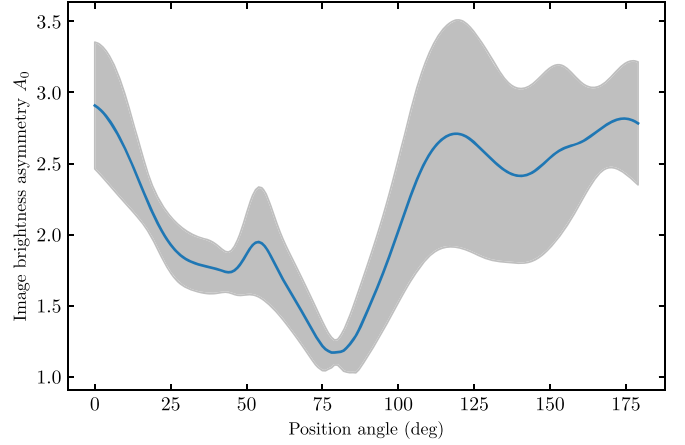
Finally, Figure 9 shows the dependence of image brightness asymmetry on the ion-to-electron temperature ratio R_{high}. As discussed earlier, changing R_{high} has a significantly smaller effect on image brightness asymmetry than the other parameters, which is within the variance seen for each model between the different image snapshots.
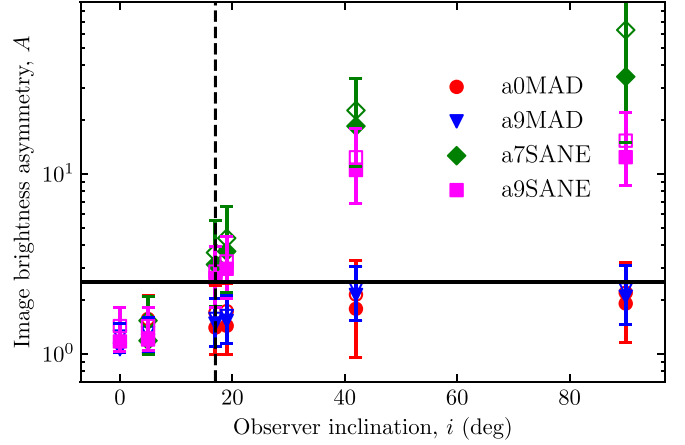
6. Implications for M87

We now consider the implications of our work for the images of M87 recently obtained by the EHT (Event Horizon Telescope Collaboration et al. 2019a). Because the EHT is a sparse interferometer, converting the interferometric data to images requires specialized algorithms with nuisance parameters, such as regularizers, that are tuned to the particular characteristics of the interferometer and the source (for details, see Event Horizon Telescope Collaboration et al. 2019d). A number of such images have been generated, with three different imaging algorithms while exploring a wide range of values for the nuisance parameters. All images are consistent with a narrow ring of emission with properties that depend very little on the particular details of image reconstruction and possess a small north–south brightness asymmetry (Event Horizon Telescope Collaboration et al. 2019d).

In the previous sections, we showed that the maximum degree of asymmetry in a black hole image depends on the inclination of the black hole spin with respect to the observer's line of sight. In M87, there is an a priori inference of the orientation of the black hole spin based on the properties of the large scale jet. The position angle in the sky of the jet has been estimated to be 288° east of north (Walker et al. 2018), while its inclination has been inferred to be 17° with respect to our line of sight (Walker et al. 2018). It is likely that the spin axis of the black hole is aligned with the large scale jet (see, however, Chatterjee et al. 2020 for a discussion of jet alignment in the case of tilted disks). In this section, we compare this information to the asymmetry properties of the EHT images. Our aim is not to show that a different inclination angle is more likely for the case of M87 but rather to ask whether low inclination is required in general to explain the low asymmetry seen in the images.

In order to compare the results of our simulations to the outcome of the observations, we apply our image brightness asymmetry measure to a fiducial set of reconstructed EHT images. Figure 10 shows the dependence of the brightness asymmetry on the position angle of the cross section. Our analysis did not include an in-depth exploration of the effect of image reconstruction of sparse interferometric data on image brightness asymmetry. Therefore, we caution against interpreting the detailed structure of this dependence as a measure of the position angle of the black hole spin axis but limit ourselves to only a qualitative comparison with theoretical expectations. The mean asymmetry for the fiducial set of EHT images for a large subset of position angles is above $A = 2$ and the maximum asymmetry is $A = 2.9$; we choose $A = 2.5$ as a representative value.

Figure 10. Mean image brightness asymmetry (blue curve) for a set of EHT M87 images as a function of the position angle of the cross section used to measure asymmetry. The 68th percentile contours are shown in gray. We define position angle as the angle east of north such that 0° corresponds to a north–south cross section. Note that there is a degeneracy between cross sections with position angles θ and $\theta + 180°$ because the asymmetry is defined to be above unity.

Figure 11. Image brightness asymmetry as a function of inclination angle i for simulations with $R_{high} = 20$, $n_{e,0} = 5 \times 10^5 \mathrm{cm}^{-3}$, and a black hole mass of $M_{BH} = 6.5 \times 10^9 M_\odot$. The simulation images have been filtered with a Butterworth filter that removes most power above $8G\lambda$ before calculating the asymmetry ratio for a better comparison with EHT images. The black line at brightness asymmetry of 2.5 shows the approximate asymmetry in the set of M87 images reconstructed from the 2017 EHT observations. The vertical dashed line corresponds to the ~17° inclination of the M87 jet. Even though both SANE and MAD models are consistent with the observed brightness asymmetry at this inclination, MAD models would have been able to reproduce such a low asymmetry even when viewed edge on.

We ran a new, focused set of simulations with parameters that are appropriate for M87. Specifically, we set the black hole mass to $M_{BH} = 6.5 \times 10^9 M_\odot$, added an intermediate inclination value of $i = 17°$, and probed electron number density scales in the range $n_{e,0} = 10^5 – 10^6 \mathrm{cm}^{-3}$ (see Chan et al. 2015 for a description of these parameters). For this new set of tailored simulations, we also applied a Butterworth filter to the images, which suppresses power above $8G\lambda$, the length of the longest EHT baseline (see Psaltis et al. 2020a for details on this filter). This allows a more direct comparison with the observed images.

In Figure 11, we plot the image brightness asymmetry as a function of the observer inclination obtained from this simulation library and compare this to the representative value

of the asymmetry in the M87 images. It is clear from this figure that, even though both SANE and MAD models are consistent with the observed brightness asymmetry at the inferred 17° inclination of the M87 black hole, MAD models would have been able to reproduce such a low asymmetry even when viewed edge on. This argues against using the image symmetry as a direct probe of observer inclination with respect to the black hole spin.

7. Summary

The images of black holes generated by the EHT have a number of coarse-scale properties that can lead to general inferences about the black holes and their accretion flows that are only marginally model dependent. For example, the size of the bright emission ring has been used to infer the mass of the black hole and test the predictions of the theory of general relativity (Event Horizon Telescope Collaboration et al. 2019f; Psaltis et al. 2020b). In the same spirit, the presence of a brightness asymmetry around the emission ring has been used in the past as an indication of the observer inclination with respect to the angular momentum of the accretion flow, and perhaps, of the black hole itself; it has been applied both to early observations of Sgr A* (Psaltis et al. 2015) as well as to the most recent images of the black hole in the center of M87 (Event Horizon Telescope Collaboration et al. 2019e).

In this paper, we explored how image brightness asymmetry is related to various black hole and model parameters and reevaluate the early argument that images with low asymmetry can only be generated in sources viewed at low inclinations, i.e., nearly face on. We use a large suite of GRMHD simulations to find explicit counterexamples to this argument, in which images with low brightness asymmetry are generated even for high observer inclinations in models that have accumulated substantial magnetic flux close to the black hole horizon, i.e., the so-called MADs. The weak brightness asymmetry in these models is a consequence of the fact that the magnetic stresses significantly decrease the angular velocity of the plasma in the inner accretion flow, and therefore, also the effects of relativistic Doppler beaming and boosting. In particular, we show that low-spin MAD models have the lowest brightness asymmetry, generating nearly uniform ring images surrounding the black hole shadows.

ORCID iDs

Lia Medeiros ⓘ https://orcid.org/0000-0003-2342-6728
Chi-Kwan Chan ⓘ https://orcid.org/0000-0001-6337-6126
Ramesh Narayan ⓘ https://orcid.org/0000-0002-1919-2730

References

Abramowicz, M. A., Calvani, M., & Nobili, L. 1980, ApJ, 242, 772
Avara, M. J., McKinney, J. C., & Reynolds, C. S. 2016, MNRAS, 462, 636
Bozza, V., de Luca, F., & Scarpetta, G. 2006, PhRvD, 74, 063001
Bronzwaer, T., Davelaar, J., Younsi, Z., et al. 2021, MNRAS, 501, 4722
Chan, C.-k., Psaltis, D., & Özel, F. 2013, ApJ, 777, 13
Chan, C.-K., Psaltis, D., Özel, F., Narayan, R., & Sądowski, A. 2015, ApJ, 799, 1
Chatterjee, K., Younsi, Z., Liska, M., et al. 2020, MNRAS, 499, 362
Do, T., Hees, A., Ghez, A., et al. 2019, Sci, 365, 664
Event Horizon Telescope Collaboration, Akiyama, K., Alberdi, A., et al. 2019a, ApJL, 875, L1
Event Horizon Telescope Collaboration, Akiyama, K., Alberdi, A., et al. 2019b, ApJL, 875, L2
Event Horizon Telescope Collaboration, Akiyama, K., Alberdi, A., et al. 2019c, ApJL, 875, L3
Event Horizon Telescope Collaboration, Akiyama, K., Alberdi, A., et al. 2019d, ApJL, 875, L4
Event Horizon Telescope Collaboration, Akiyama, K., Alberdi, A., et al. 2019e, ApJL, 875, L5
Event Horizon Telescope Collaboration, Akiyama, K., Alberdi, A., et al. 2019f, ApJL, 875, L6
Event Horizon Telescope Collaboration, Akiyama, K., Algaba, J. C., et al. 2021a, ApJL, 910, L12
Event Horizon Telescope Collaboration, Akiyama, K., Algaba, J. C., et al. 2021b, ApJL, 910, L13
Gammie, C. F., McKinney, J. C., & Tóth, G. 2003, ApJ, 589, 444
Gravity Collaboration, Abuter, R., Amorim, A., et al. 2020, A&A, 636, L5
Gravity Collaboration, Abuter, R., Amorim, A., et al. 2021, A&A, 647, A59
Igumenshchev, I. V., Abramowicz, M. A., & Novikov, I. D. 1998, MNRAS, 298, 1069
Igumenshchev, I. V., Narayan, R., & Abramowicz, M. A. 2003, ApJ, 592, 1042
Johannsen, T., & Psaltis, D. 2010, ApJ, 718, 446
Medeiros, L., Psaltis, D., & Özel, F. 2020, ApJ, 896, 7
Mościbrodzka, M., Falcke, H., & Shiokawa, H. 2016, A&A, 586, A38
Narayan, R., Sądowski, A., Penna, R. F., & Kulkarni, A. K. 2012, MNRAS, 426, 3241
Özel, F., Psaltis, D., & Narayan, R. 2000, ApJ, 541, 234
Psaltis, D., & Johannsen, T. 2012, ApJ, 745, 1
Psaltis, D., Medeiros, L., Christian, P., et al. 2020b, PhRvL, 125, 141104
Psaltis, D., Medeiros, L., Lauer, T. R., Chan, C.-K., & Ozel, F. 2020a, arXiv:2004.06210
Psaltis, D., Narayan, R., Fish, V. L., et al. 2015, ApJ, 798, 15
Rybicki, G. B., & Lightman, A. P. 1986, Radiative Processes in Astrophysics (New York: Wiley)
Sądowski, A., Narayan, R., Penna, R., & Zhu, Y. 2013, MNRAS, 436, 3856
Satapathy, K., Psaltis, D., & Ozel, F. 2021, arXiv:2111.01317
Walker, R. C., Hardee, P. E., Davies, F. B., Ly, C., & Junor, W. 2018, ApJ, 855, 128
Younsi, Z., Wu, K., & Fuerst, S. V. 2012, A&A, 545, A13
Yuan, F., & Narayan, R. 2014, ARA&A, 52, 529